Applied Thermal Engineering 100 (2016) 1119–1129

Contents lists available at ScienceDirect

Applied Thermal Engineering

journal homepage: www.elsevier.com/locate/apthermeng

Research Paper

Performance analysis of a novel expansion valve and control valves designed for a waste heat-driven two-adsorber bed adsorption cooling system

Amir Sharafian *, Patric Constantin Dan, Wendell Huttema, Majid Bahrami *

Laboratory for Alternative Energy Conversion (LAEC), School of Mechatronic Systems Engineering, Simon Fraser University, Surrey, BC, Canada V3T 0A3

HIGHLIGHTS

- New ideas for the expansion and control valves of adsorption cooling systems are proposed.
- A two-bed silica gel/$CaCl_2$-water adsorption cooling system is built to test the new ideas.
- The control valves are 10.5 kg lighter than other available designs in the literature.
- The control valve arrangements result in 50% less parasitic power consumption in one cycle.
- A check valve with cracking pressure of 3.5–7 kPa is proposed for the expansion valve.

ARTICLE INFO

Article history:
Received 8 August 2015
Accepted 28 February 2016
Available online 7 March 2016

Keywords:
Expansion valve
Control valve
Adsorption cooling system
Silica gel/$CaCl_2$
Vehicle air conditioning

ABSTRACT

Two new ideas for the expansion valve and control valves of an adsorption cooling system (ACS) for vehicle air conditioning applications are suggested to reduce its weight and parasitic power consumption, and simplify its control system. A check valve with cracking pressure of 3.5–7 kPa is proposed for the expansion valve and a combination of low cracking pressure check valves and solenoid valves with an innovative arrangement is proposed for the control valves. These new designs are installed on a two-adsorber bed silica gel/$CaCl_2$-water ACS and tested under different operating conditions. These designs result in reducing the total mass of the ACS up to 10.5 kg and the parasitic power consumption of the control valves by 50%. The results show that the expansion valve and control valves operate effectively under the heating and cooling fluid inlet temperatures to the adsorber beds of 70–100 °C and 30–40 °C, respectively, the coolant water inlet temperature to the condenser of 30–40 °C, and the chilled water inlet temperature to the evaporator of 15–20 °C. Also, an ACS thermodynamic cycle model is developed and compared against the experimental data for prediction and further improvement of the ACS performance. The results of the numerical modeling show that by increasing the adsorber bed heat transfer coefficient and surface area, the specific cooling power of the system increases up to 6 times.

1. Introduction

Waste heat-driven driven adsorption cooling systems (ACS) are potential energy efficient replacements for vapor compression refrigeration cycles (VCRC) in vehicles' air conditioning (A/C) applications. An ACS utilizes a low grade thermal energy to generate cooling power required in a vehicle. Approximately 70% of the total fuel energy released in an internal combustion engine (ICE) is wasted as heat that is dissipated through the engine coolant and exhaust gas [1]. An ACS can use this wasted heat to provide cooling in vehicles and drastically reduce the vehicle's fuel consumption and carbon footprint.

An ACS uses an adsorbent–adsorbate working pair, where the adsorbate, such as water or methanol, is adsorbed and desorbed from the surface of the adsorbent, such as zeolite, silica gel, or activated carbon, in a waste heat-driven cycle. Most of these materials are nontoxic, noncorrosive, and inexpensive [2] making ACS a safe and environmentally friendly technology. An ACS operates more quietly than a VCRC and is easier to maintain because its only moving parts are valves [3]. However, current ACS are limited in their usefulness for commercial vehicle applications, specifically light-duty vehicles, because of their bulkiness and heavy weight which are due to the low thermal conductivity of adsorbent materials and the low mass diffusivity of adsorbent–adsorbate pairs. These properties result in a low coefficient of performance (COP = cooling energy/input energy) and low specific cooling power (SCP = cooling energy/(adsorbent mass × cycle time)). In vehicle applications, the

* Corresponding authors. Tel.: +1 778 782 8538; fax: +1 778 782 7514.
E-mail addresses: asharafi@sfu.ca (A. Sharafian), mbahrami@sfu.ca (M. Bahrami).

http://dx.doi.org/10.1016/j.applthermaleng.2016.02.118
1359-4311/

Table 1
Performance analysis of different finned tube adsorber beds reported in the literature.

Ref. no.	Adsorber bed type	Working pairs	Control valves on adsorber beds	Control valves on heating/cooling sys.
[18]	1 SS 304 annulus tube HEX	Consolidated natural graphite + zeolite 13X/water	4 electrically actuated valves	4 electrically actuated valves
[19]	2 annulus tube HEX	Consolidated zeolite/water	4 pneumatic vacuum valves	8 electrically actuated valves
[20–26]	2 plate-tube HEX	Act. carbon/ammonia	4 check valve	12 valves
[27,28]	2 shell and tube HEX	Act. carbon/methanol	4 magnetic vacuum valves	10 hand ball valves
[29]	4 shell and tube HEX	Act. carbon/ammonia	14 valves	16 valves
[30–34]	SS simple tube	Consolidated act. carbon/ammonia	No valve	No valve
[35–38]	Plate HEX	Consolidated act. carbon/ammonia	4 check valves + 2 solenoid valves	4 three-way valves
[39]	4 plate HEX	Silica gel/water	8 solenoid valves	20 solenoid valves
[40,41]	4 plate fin HEX	Silica gel/water	10 pressure relief valves	16 valves
[42–44]	2 plate fin HEX	Silica gel/water	No valve	11 solenoid valves
[45]	2 plate fin HEX	Silica gel/water	4 solenoid valves	Manual hand ball valves
[46]	1 flat-tube HEX with corrugated fins	Silica gel/water	No valves	4 three-way valves
[47–49]	1 aluminum finned tube HEX	Consolidated activated carbon/ammonia	4 check valves	10 shut-off valves
[50]	1 SS finned tube HEX	Silica gel/methanol	2 hand ball valves	4 three-way valves
[51–53]	SS Cylindrical double finned tube HEX	Zeolite 13X/water	3 manual vacuum valves	4 manual hand ball valves
[7,8]	1 finned tubes HEX	Zeolite 13X/water	4 vacuum valves	3 check valves
[54]	1 SS finned tube HEX	silica gel + $CaCl_2$ (SWS-1L)/water	2 vacuum valves	2 three-way valves
[55]	2 Aluminum finned tube HEX	AQSOA FAM-Z02/water	4 check valves + 1 hand ball valve	–
[56–58]	2 finned tube HEX	Silica gel/water	1 solenoid vacuum valve	11 solenoid valves
[59]	1 SS finned tube HEX	Coated hydrophobic Y zeolite (CBV-901)/methanol	2 vacuum valves	2 three-way valves
[60]	2 finned tube HEX	Silica gel/water	1 solenoid vacuum valve	11 solenoid valves
[61–64]	2 finned tube HEX	Act. carbon + $CaCl_2$ (1:4)/ammonia	4 hand ball valves	Hand ball valves
[65]	1 aluminum finned tube HEX	Silica gel + $CaCl_2$ (SWS-1L)/water	2 vacuum valves	2 three-way valves
[66]	Finned tube HEX	Silica gel + $CaCl_2$/water	No valve	–
[14–17]	2 Aluminum finned tube HEX	Silica gel/water	4 check valves	4 three-way valves
[67–69]	1 aluminum finned tube HEX	$LiNO_3$-Silica KSK/water	2 vacuum valves	4 solenoid valve + 4 check valves
[70,71]	28 finned tube with 2.5 mm fin spacing	Silica gel + LiCl/water	1 solenoid vacuum valve	11 solenoid valves
[72–74]	2 aluminum finned tube HEX	Silica gel + LiCl/methanol Silica gel/water	1 solenoid vacuum valve	11 solenoid valves
[75]	2 aluminum finned tube HEX	AQSOA FAM-Z02/water	4 electrically actuated valves	Solenoid valves
[76,77]	8 HEX with aluminum fins + steel pipes	Expanded graphite + $CaCl_2$/ammonia Expanded graphite + $BaCl_2$/ammonia	4 valves 1 solenoid vacuum valve	8 valves 11 solenoid valves
[78]	1 carbon steel finned tube HEX	Expanded graphite + NaBr/ammonia	2 valves	4 valves
[79]	4 SS shell and aluminum finned tube HEX	Silica gel/water	8 electrically actuated valves	16 electrically actuated valves
[80]	2 finned tube HEX	Expanded graphite + $CaCl_2$/ammonia	No valve	3 three-way valves
[81]	2 copper finned tube HEX	Zeolite 13X + $CaCl_2$/water	6 solenoid valves	10 solenoid valves

SS, stainless steel.
HEX, heat exchanger.

mass of auxiliary systems should be minimized. Therefore, the SCP becomes an important parameter in a mobile ACS design [4].

Sharafian and Bahrami [5] conducted a comprehensive literature review on the feasibility of ACS installation in light-duty vehicles, different ACS thermodynamic cycle modeling, and practical examples of ACS installed in vehicles such as a refrigerated rail car with two-adsorber bed silica gel-sulphur dioxide ACS [6], a locomotive with waste heat-driven single-adsorber bed zeolite 13X-water ACS [7,8], and a fishing boat with waste heat-driven two-adsorber bed consolidated activated carbon/$CaCl_2$-ammonia ACS for ice production [9–13]. These examples were successful ACS installed in vehicle applications where the weight and footprint of the ACS were not problematic. For light-duty vehicle A/C applications, de Boer et al. [14–17] built and installed a two-adsorber bed silica gel-water ACS with 2-kW cooling power on a compact car, Fiat Grande Punto. In their setup, each adsorber bed was filled with 3 kg of silica gel with the adsorber bed to adsorbent mass ratio (AAMR) of 4.2 $kg_{metal}/kg_{dry\ adsorbent}$. The 86 kg total mass of their system exceeded the 35 kg limit set by the car manufacturer [14]. From the data reported in Refs. [14,15], one can conclude that the mass of the two adsorber beds loaded with adsorbent material was 31.2 kg (2 adsorber beds × (3 $kg_{dry\ adsorbent}$ + 4.2 $kg_{metal}/kg_{dry\ adsorbent}$ × 3 $kg_{dry\ adsorbent}$)) which made only 36% of the total mass of the system. The condenser, evaporator, expansion valve, piping and control valves contributed the remaining 64% of the ACS total mass. This shows that the mass of all components not only adsorber beds became important for vehicle A/C applications. Table 1 shows the details of different waste heat-driven ACS including adsorber bed type, working pairs, and number and type of control valves.

The valves installed on an ACS for vehicle applications should be automated. It can be seen in Table 1 that the best choice for the valves installed between the adsorber beds, and condenser and evaporator are check valves. These valves have no power consumption and operate by the pressure difference between the two sides of the valve. Also, Table 1 indicates that electrically actuated ball valves and solenoid valves are installed on the most of ACS experiments to control the heating and cooling systems automatically. Solenoid valves are lighter than electrically actuated ball valves and have faster response. However, they have higher electricity power consumption than electrically actuated ball valves. Our analysis showed that the power consumption and complexity of control valves have been overlooked in the literature and there is no information or strategy to minimize the parasitic power consumption of the valves.

In ACS stationary applications that used water as the refrigerant, an inverse U-bend tubing was employed as an expansion valve. However, the constant height of the U-bend tubing limited its operating range. For vehicle applications, where the A/C system experiences different ambient temperatures, this type of expansion valves cannot operate effectively. To this end, we proposed a new design for the expansion valve of an ACS to meet the requirements of a well-designed ACS for vehicle applications.

In the present study, two ideas are proposed for the expansion valve and control valves of an ACS for vehicle A/C applications to simplify the control system, and reduce the total mass of the ACS and the parasitic power consumption of the control valves. As a proof-of-concept demonstration, a two-adsorber bed silica gel/$CaCl_2$ ACS is designed and built to test these ideas. To evaluate the functionality of the expansion and control valves, parametric studies are performed under different operating conditions. An ACS thermodynamic cycle model is also developed and compared against the experimental data for prediction and further improvement of the ACS performance. Finally, additional modifications to improve the performance of the ACA are proposed.

2. ACS thermodynamic cycle

The thermodynamic cycle of an ACS is comprised of two main steps: heating–desorption–condensation and cooling–adsorption–evaporation. With a single adsorber bed, an ACS generates evaporative cooling power intermittently. To produce a continuous cooling power, one must use more than one adsorber bed. Fig. 1a depicts a schematic of a typical two-adsorber bed ACS comprised of two adsorber beds, a condenser, an expansion valve, and an evaporator.

Fig. 1b shows the thermodynamic processes in an ACS which is divided into two subcycles: (i) an adsorbent cycle (on the right side), and (ii) an adsorbate cycle (on the left side). As shown in Fig. 1b, the adsorbent cycle includes four steps: (1) isosteric heating (ih); process 1–2, (2) isobaric desorption (ibd); process 2–3', (3) isosteric cooling (ic); process 3'–4', and (4) isobaric adsorption (iba); process 4'–1. Isosteric processes occur at constant specific volume and isobaric processes occur at constant pressure. The adsorbate cycle shown in Fig. 1b includes three steps: (1) isobaric condensation in the condenser; process 2–3, (2) isenthalpic process in the expansion valve; process 3–4, and (3) isobaric evaporation in the evaporator; process 4–1.

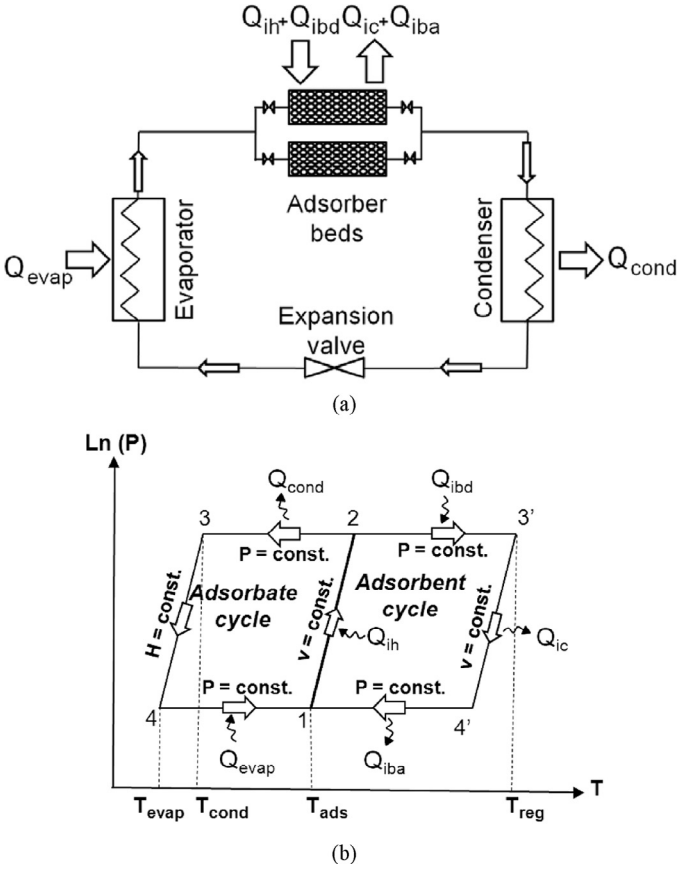

Fig. 1. (a) Schematic and (b) thermodynamic cycle of a two-adsorber bed ACS [82].

During step 1–2, the adsorbent-adsorbate pair absorbs heat of Q_{ih} from an external heat source in an isosteric process. In this step, temperature and pressure of the adsorber bed increase due to the adsorbate desorption from the adsorbent particles. This process is continued until the pressure of the adsorber bed reaches the pressure of the condenser and the inlet valve to the condenser is opened. In step 2–3', the external heat source continuously heats the adsorber bed (Q_{ibd}) during an isobaric desorption process, the adsorbate leaves the adsorber bed, and is condensed inside the condenser through an isobaric cooling process (steps 2–3). Upon reaching the point 3', the maximum temperature of the cycle, the valve between the adsorber bed and the condenser is closed, and during an isosteric cooling process (step 3'–4'), the temperature of the adsorbent is reduced by dissipating the heat of Q_{ic} through a heat sink. In steps 3–4, the adsorbate inside the condenser passes through the expansion valve and enters to the evaporator. During steps 4–1, the adsorbate absorbs the heat of Q_{evap} from the environment of interest and evaporates. At the same time, the valve between the evaporator and the adsorber bed is opened and the adsorbent adsorbs the vaporous adsorbate through an isobaric adsorption process (step 4'–1) and releases heat of Q_{iba}.

3. Experimental study

An ACS with more than 60 different components was designed and built to test the proposed ideas. Fig. 2a–c shows a schematic of the two-adsorber bed waste heat-driven ACS along with photos of the system components. The ACS equipped with four temperature control systems (TCS) to control the adsorption and desorption temperatures in the adsorber beds, and the condensation and evaporation temperatures in the condenser and evaporator, respectively. As shown in Fig. 2a, valves V1–V4 are installed before and after the adsorber beds to control the adsorption and desorption processes, and eight valves (V5–V12) are installed on the TCSs (TCS_{HF} and TCS_{CF}) to intermittently heat and cool adsorber beds 1 and 2.

Silica gel/$CaCl_2$ adsorbent material was prepared with combining chromatography-grade commercial silica gel with irregular-shaped grains (0.5–1.0 mm) and average pore diameter of 5.7 nm (SiliaFlash N60, Silicycle Inc.) with 30% wt. $CaCl_2$. Two heat exchangers, as shown in Fig. 2d, were designed and built based on the results of Sharafian et al. [83] to be packed with the silica gel/$CaCl_2$ composite adsorbent. Type T thermocouples (Omega, model #5SRTC-TT-T-36-36) with accuracy of 0.75% of reading and pressure transducers (Omega, model #PX309-005AI) with 0–34.5 kPa operating range and ±0.4 kPa accuracy were used to monitor and record the temperature and pressure variations in each component of the ACS over time.

Four check valves, V1–V4, were installed to reduce the weight and electrical power consumption of the ACS, and to simplify its control system. The check valves between the adsorber beds and the condenser, and the adsorber beds and the evaporator must have a low cracking pressure. An ACS which uses water as the refrigerant operates between 1 and 8 kPa, therefore any pressure drop between the adsorber beds and the condenser or the adsorber beds and the evaporator reduces the system performance. In this study, the check valves (Generant, model #DCV-375B-S) have a cracking pressure of less than 250 Pa, have no power consumption, and are durable and inexpensive.

To control the heating and cooling of the adsorber beds, eight solenoid valves, V5–V12, (StcValve, model #2W160-1/2-3-V with 14 W power consumption and #2WO160-1/2-3-V with 30 W power

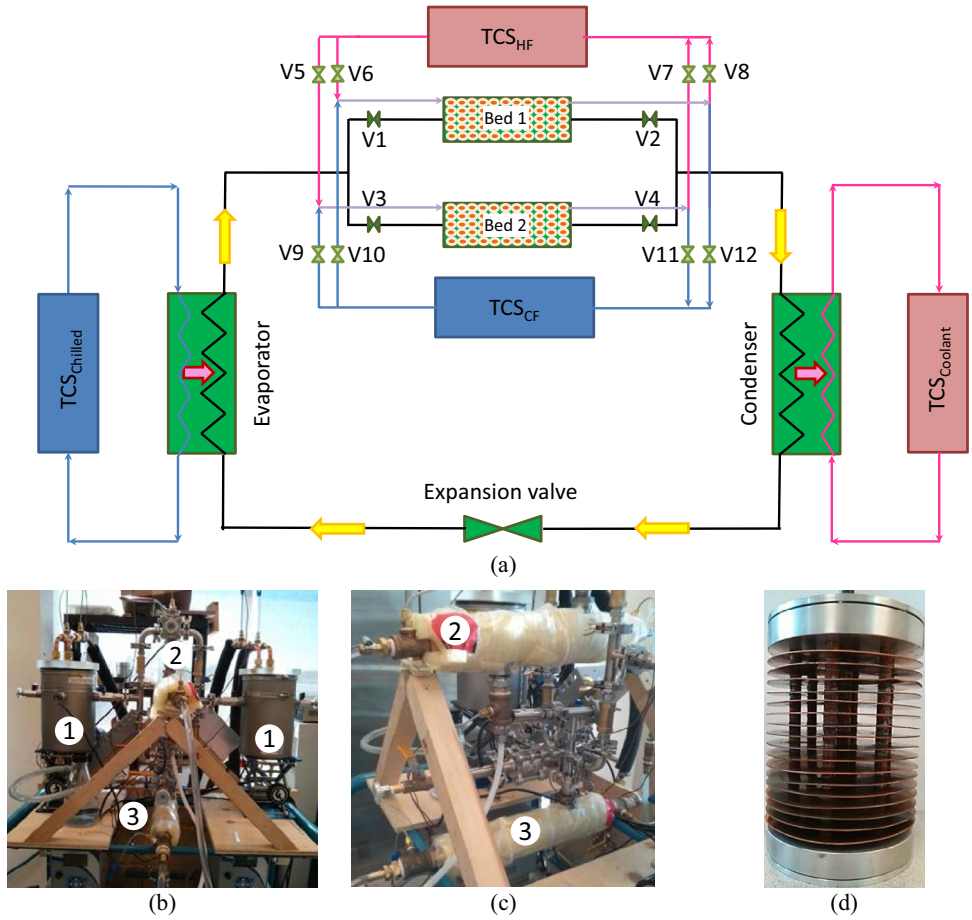

Fig. 2. (a) Schematic of a two-adsorber bed ACS, (b–c) ACS components: 1 – adsorber beds, 2 – condenser, and 3 – evaporator, and (d) custom-built heat exchanger located inside the adsorber beds.

consumption) with a maximum operating temperature of 120 °C and a total power consumption of 176 W were installed. The solenoid valve arrangements for the heat transfer fluid header and collector of the ACS are displayed in Fig. 3.

As shown in Fig. 3, solenoid valves V5, V7, V10, and V12 are normally closed and solenoid valves V6, V8, V9, and V11 are normally open. To desorb adsorber bed 1, heating fluid comes from TCS_{HF}, enters the header, passes through valve V6, and goes to adsorber bed 1, as shown in Fig. 3a, and then returns from adsorber bed 1, passes through valve V8, and returns to TCS_{HF}, as shown in Fig. 3b. For the adsorption process in adsorber bed 2, cooling fluid comes from TCS_{CF}, passes through valve V9, and enters adsorber bed 2. Then, it returns from adsorber bed 2, passes through valve V11, and returns to TCS_{CF}. When the solenoid valves are not energized, TCS_{HF} and TCS_{CF} are connected to adsorber beds 1 and 2, respectively. When the solenoid valves are energized, the flow directions of heating and cooling fluids are switched, and TCS_{HF} and TCS_{CF} are connected to adsorber bed 2 and 1, respectively.

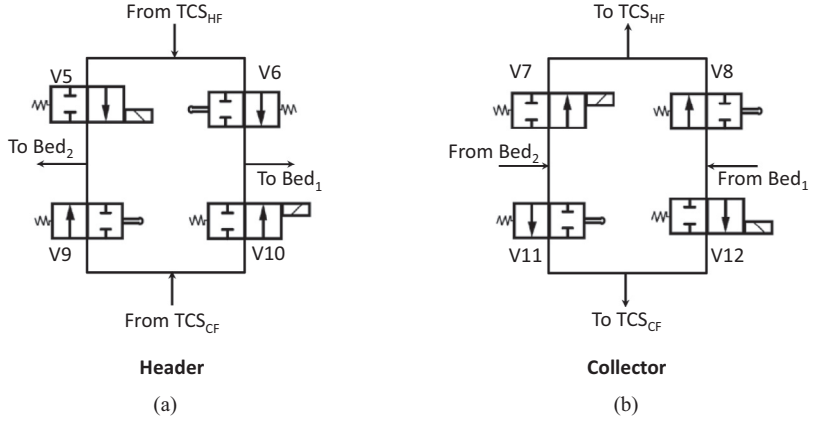

Fig. 3. Solenoid valve arrangements in (a) the header and (b) collector of the two-adsorber bed ACS. : normally opened, : normally closed.

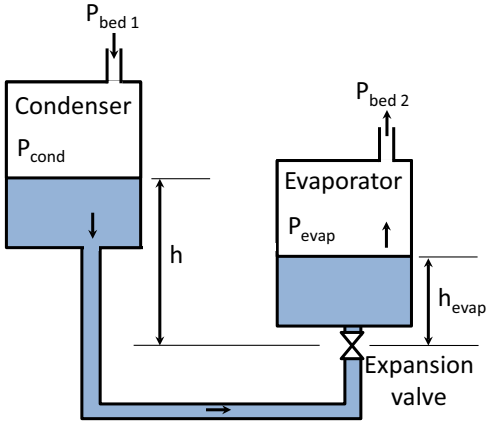

Fig. 4. Schematic of the proposed expansion valve for a waste heat-driven ACS.

With this design, valves V1–V8 are controlled with only a relay switch, which in turn is controlled automatically using a LabVIEW program, and the power consumption of valves V1–V8 for one cycle reduces by 50%. Also, check valves V1–V4 operate automatically, without power consumption, actuated by the pressure gradients between the adsorber beds, and the condenser and the evaporator. The total mass of the eight solenoid valves and four check valves is about 7 kg (8×0.815 kg + 4×0.115 kg). If electrically or pneumatically actuated ball valves were used, the total mass of eight valves and four check valves of the same size would be 17.5 kg (8×2.130 kg + 4×0.115 kg) which is 10.5 kg (2.5 times) heavier than the design in this study.

The expansion valve of a refrigeration system prevents the vaporous refrigerant in the condenser from flowing to the evaporator, and creates a pressure difference between the condenser and evaporator that is set by the refrigerant saturation pressure. Therefore, the expansion valve of an ACS that uses water as the refrigerant (adsorbate) differs from those of designed for conventional VCRCs that use commercial refrigerants such as chlorofluorocarbons (CFCs), hydrochlorofluorocarbons (HCFCs), and hydrofluorocarbons (HFCs). Among ACS experiments for stationary applications, a reverse U-bend tube was used as the expansion valve such as the one reported in Ref. [84]. The problem associated with a reverse U-bend tube in an ACS that uses water as the refrigerant is its fixed height. To create a pressure drop of 5 kPa between the condenser and evaporator, the height of such a reverse U-bend is about 50 cm which is not practical for light-duty vehicle A/C applications and limits the operating range of the ACS. In this study, to resolve the issue of U-bend tube for vehicle applications and design an expansion valve for a wide range of operating conditions, a check valve (Generant, model #CV-250B-S-1) with a cracking pressure of 3.4–6.9 kPa is proposed.

Fig. 4 shows the positions of the condenser and evaporator, and the expansion valve located between them. The condensed refrigerant (adsorbate) is accumulated at the outlet of the condenser and before the expansion valve. As such, the hydrostatic pressure balance for the fluid between the condenser and evaporator is used to relate P_{cond} and P_{evap} to the cracking pressure of the check valve ($P_{cracking}$):

$$P_{\mathrm{cond}} - P_{\mathrm{evap}} - \rho g h_{\mathrm{evap}} + \rho g h > P_{\mathrm{cracking}} \tag{1}$$

Eq. (1) shows that the expansion valve connects the condenser to the evaporator only if the sum of the left-side terms becomes larger than the cracking pressure of the check valve, $P_{cracking}$. As such, the term ρgh in Eq. (1) created by the accumulation of liquid refrigerant (adsorbate) at the outlet of the condenser guarantees that no vaporous refrigerant passes through the expansion valve. Such a compact expansion valve can effectively operate in a vehicle where operating conditions vary significantly and vibrations are abundant. The other specifications of the designed ACS and the operating conditions are summarized in Table 2.

Table 2
Specifications and operating conditions of the ACS built in this study.

Parameter	Changed values
Working pairs	Silica gel/$CaCl_2$-water
Mass of adsorbent per adsorber bed (kg)	1.15
Metal mass of adsorber bed (kg)	2.8
Adsorber bed heat transfer surface area, A_{bed} (m^2)	0.235
Adsorber bed heat transfer coefficient, U_{bed} (W/m^2K)	20.0
Heating fluid mass flow rate to adsorber bed (kg/s)	0.058 (4.1 L/min of silicone oil)
Cooling fluid mass flow rate to adsorber bed (kg/s)	0.062 (4.1 L/min of silicone oil)
Heat capacity of silicone oil (kJ/kgK)	1.8
Metal mass of condenser (kg)	1.9
Condenser heat transfer surface area, A_{cond} (m^2)	0.1444
Condenser heat transfer coefficient, U_{cond} (W/m^2K)	250
Coolant water mass flow rate to condenser (kg/s)	0.036 (2.16 L/min of water)
Metal mass of evaporator (kg)	1.9
Evaporator heat transfer surface area, A_{evap} (m^2)	0.072
Evaporator heat transfer coefficient, U_{evap} (W/m^2K)	250
Chilled water mass flow rate to evaporator (kg/s)	0.02 (1.2 L/min of water)
Heating fluid inlet temperature (°C)	90
Cooling fluid inlet temperature (°C)	30
Coolant fluid inlet temperature (°C)	30
Chilled water inlet temperature (°C)	15

4. Numerical modeling

A dynamic lumped-body model was developed for the ACS thermodynamic cycle to predict the performance of the system and further improve the design. The energy balance on the adsorber bed during the isosteric heating (process 1–2 in Fig. 1b) is expressed as follows:

$$m_{adsorbent}\left[c_{adsorbent}+c_{p,liq.\,adsorbate}\omega_{max}+c_{bed}\frac{m_{bed}}{m_{adsorbent}}\right]\frac{dT_{adsorbent}}{dt} = U_{bed}A_{bed}\Delta T_{LM,bed} \tag{2}$$

where $m_{adsorbent}$ is the mass of dry adsorbent and $\frac{m_{bed}}{m_{adsorbent}}$ is the AAMR. In Eq. (2), $T_{adsorbent}$ is the adsorbent particles temperature and ω_{max} is the maximum adsorbate uptake at the adsorbent temperature and evaporator pressure, see Fig. 1b. U_{bed} and A_{bed} are the overall heat transfer coefficient and heat transfer surface area of the adsorber bed, respectively. $\Delta T_{LM,bed}$ defines the adsorber bed log mean temperature difference (LMTD) between the adsorbent particles and heating fluid:

$$\Delta T_{LM,bed} = \frac{T_{hf,i}-T_{hf,o}}{\ln\left(\frac{T_{hf,i}-T_{adsorbent}}{T_{hf,o}-T_{adsorbent}}\right)} \tag{3}$$

where $T_{hf,i}$ and $T_{hf,o}$ are the heating fluid inlet and outlet temperatures. Eq. (4) gives the heating fluid outlet temperature during the isosteric heating process:

$$\dot{m}_{hf}c_{p,hf}\left(T_{hf,i}-T_{hf,o}\right) = U_{bed}A_{bed}\Delta T_{LM,bed} \tag{4}$$

where $\dot{m}_{hf}$ is the heating fluid mass flow rate. During the isobaric desorption (process 2–3' in Fig. 1b), the energy balance on the

adsorber bed and the adsorbate uptake rate by the adsorbent particles are expressed as follows:

$$m_{adsorbent}\left[c_{adsorbent}+c_{p,liq.\,adsorbate}\omega+c_{bed}\frac{m_{bed}}{m_{adsorbent}}\right]\frac{dT_{adsorbent}}{dt} - m_{adsorbent}\frac{d\omega}{dt}\Delta h_{ads}=U_{bed}A_{bed}\Delta T_{LM,bed} \quad (5)$$

$$\frac{d\omega}{dt}=\frac{15D_s}{R_p^2}(\omega_{eq}-\omega) \quad (6)$$

The first and second terms in the left-hand side of Eq. (5) represent the sensible and latent heats, respectively. Eq. (6) gives the adsorbate uptake rate, $\frac{d\omega}{dt}$, which is a function of the solid-side mass diffusivity, D_s, the average radius of the adsorbent particles, R_p, and the equilibrium adsorbate uptake of the adsorbent particles, ω_{eq}. The solid-side mass diffusivity is expressed as $D_{s0}\exp(-E_a/R_uT_{adsorbent})$, where D_{s0} is the pre-exponential constant, E_a is the activation energy, and R_u is the universal gas constant. In this study, the adsorbent material is silica gel/$CaCl_2$ and the constant values of D_{s0}, E_a, and R_p are 2.54×10^{-4} m^2/s, 42.0 kJ/mol, and 0.375×10^{-3} m, respectively [85,86]. Eq. (7) gives the equilibrium water uptake by silica gel/$CaCl_2$ [85,86]:

$$\omega_{eq}=\frac{\omega_m K_0\exp\left(\frac{\Delta h_{ads}M_{adsorbate}}{R_uT_{adsrobent}}\right)P}{\left[1+\left[K_0\exp\left(\frac{\Delta h_{ads}M_{adsorbate}}{R_uT_{adsrobent}}\right)P\right]^n\right]^{1/n}} \quad (7)$$

where P, $M_{adsorbate}$ and Δh_{ads} are the operating pressure in mbar, the molar mass of adsorbate, and the enthalpy of adsorption, respectively. For silica gel/$CaCl_2$-water, Δh_{ads}, K_0, ω_m, and n are equal to 2760 kJ/kg, 2.0×10^{-10} mbar^{-1}, 0.8 kg/kg, and 1.1, respectively [85,86]. The energy balance on the condenser is expressed by Eqs. (8)–(10):

$$-m_{adsorbate}\frac{d\omega}{dt}\left[h_{fg,adsorbate@T_{cond}}+c_{p,vaporous\,adsorbate}(T_{adsorbent}-T_{cond})\right] - U_{cond}A_{cond}\Delta T_{LM,cond}=m_{cond}c_{cond}\frac{dT_{cond}}{dt} \quad (8)$$

$$\Delta T_{LM,cond}=\frac{T_{coolant,i}-T_{coolant,o}}{\ln\left(\frac{T_{cond}-T_{coolant,o}}{T_{cond}-T_{coolant,i}}\right)} \quad (9)$$

$$\dot m_{coolant}c_{p,coolant}(T_{coolant,o}-T_{coolant,i})=U_{cond}A_{cond}\Delta T_{LM,cond} \quad (10)$$

where $T_{coolant,i}$ and $T_{coolant,o}$ are the coolant fluid inlet and outlet temperatures to the condenser and h_{fg} is the enthalpy of vaporization during the condensation process. The set of Eqs. (3)–(10) should be solved simultaneously to find the adsorbent particles temperature, adsorbate uptake rate, heating fluid outlet temperature, and adsorber bed LMTD, as well as the condenser and coolant fluid outlet temperatures during the isobaric desorption and condensation processes. The amounts of heat transfer to the adsorber bed from the heat source during the isosteric heating and isobaric desorption processes, and the heat removal from the condenser during the condensation process are calculated as follows:

$$\dot q_{heating}=\dot m_{hf}c_{p,hf}(T_{hf,i}-T_{hf,o}) \quad (11)$$

$$\dot q_{cond}=\dot m_{coolant}c_{p,coolant}(T_{coolant,i}-T_{coolant,o}) \quad (12)$$

Eqs. (13)–(15) express the energy balance during the isosteric cooling (process 3'–4' in Fig. 1b). This process is similar to the isosteric heating process except the cooling fluid replaces the heating fluid.

$$m_{adsorbent}\left[c_{adsorbent}+c_{p,liq.\,adsorbate}\omega_{min}+c_{bed}\frac{m_{bed}}{m_{adsorbent}}\right]\frac{dT_{adsorbent}}{dt} = U_{bed}A_{bed}\Delta T_{LM,bed} \quad (13)$$

$$\Delta T_{LM,bed}=\frac{T_{cf,i}-T_{cf,o}}{\ln\left(\frac{T_{cf,i}-T_{adsorbent}}{T_{cf,o}-T_{adsorbent}}\right)} \quad (14)$$

$$\dot m_{cf}c_{p,cf}(T_{cf,i}-T_{cf,o})=U_{bed}A_{bed}\Delta T_{LM,bed} \quad (15)$$

where ω_{min} is the minimum equilibrium adsorbate uptake in the ACS thermodynamic cycle at the end of the isobaric desorption process and is calculated at the adsorber bed temperature and condenser pressure, see Fig. 1b. The energy balance on the adsorber bed during the isobaric adsorption (process 4'–1 in Fig. 1b) is expressed as follows:

$$m_{adsorbent}\left[c_{adsorbent}+c_{p,liq.\,adsorbate}\omega+c_{bed}\frac{m_{bed}}{m_{adsorbent}}\right]\frac{dT_{adsorbent}}{dt} - m_{adsorbent}\frac{d\omega}{dt}\left[\Delta h_{ads}-c_{p,vaporous\,adsorbate}(T_{adsorbent}-T_{evap})\right] = U_{bed}A_{bed}\Delta T_{LM,bed} \quad (16)$$

The governing equations during the evaporation process are summarized in Eqs. (17)–(19):

$$-m_{adsorbate}\frac{d\omega}{dt}\left[h_{fg,adsorbate@T_{evap}}-c_{p,liq.\,adsorbate}(T_{cond}-T_{evap})\right] + U_{evap}A_{evap}\Delta T_{LM,evap}=m_{evap}c_{evap}\frac{dT_{evap}}{dt} \quad (17)$$

$$\Delta T_{LM,evap}=\frac{T_{chilled,i}-T_{chilled,o}}{\ln\left(\frac{T_{chilled,i}-T_{evap}}{T_{chilled,o}-T_{evap}}\right)} \quad (18)$$

$$\dot m_{chilled}c_{p,chilled}(T_{chilled,i}-T_{chilled,o})=U_{evap}A_{evap}\Delta T_{LM,evap} \quad (19)$$

Eqs. (6) and (14)–(19) should be solved simultaneously to find the adsorbent particles temperature and chilled water outlet temperature during the isobaric adsorption and evaporation processes, respectively. The heat removal from the adsorber bed during the isosteric cooling and isobaric adsorption processes as well as heat transfer to the evaporator during the evaporation process are calculated as follows:

$$\dot q_{cooling}=\dot m_{cf}c_{p,cf}(T_{cf,i}-T_{cf,o}) \quad (20)$$

$$\dot q_{evap}=\dot m_{chilled}c_{p,chilled}(T_{chilled,i}-T_{chilled,o}) \quad (21)$$

Eqs. (22)–(25) give the total amount of heat transfer to/removal from the adsorber beds, condenser and evaporator:

$$Q_{total\,heating}=\int_{steps\,(1\text{–}2)+(2\text{–}3')}\dot q_{heating}dt \quad (J) \quad (22)$$

$$Q_{total\,cooling}=\int_{steps\,(3'\text{–}4')+(4'\text{–}1)}\dot q_{cooling}dt \quad (J) \quad (23)$$

$$Q_{cond}=\int_{step\,(2\text{–}3)}\dot q_{cond}dt \quad (J) \quad (24)$$

$$Q_{evap}=\int_{step\,(4\text{–}1)}\dot q_{evap}dt \quad (J) \quad (25)$$

Accordingly, the COP and SCP of the ACS during one cycle are calculated:

$$COP = \frac{Q_{evap}}{Q_{total\ heating}} \tag{26}$$

$$SCP = \frac{Q_{evap}}{m_{adsorbent}\,\tau_{cycle}} \quad (W/kg) \tag{27}$$

where τ_{cycle} in Eq. (27) is the cycle time.

To solve the set of differential equations simultaneously, the Runge–Kutta–Fehlberg method (RKF45) was adopted because the governing equations in the ACS thermodynamic modeling were only a function of time. In the in-house code, the marching time step was set at 0.1 s and the relative error difference between two consequent iterations at each time step was set at 10^{-9}. Also, the absolute error difference between the results at the end of two consequent cycles was set at 10^{-3}.

5. Results and discussion

5.1. Base-case operating condition

Fig. 5 shows the performance of the ACS with a new expansion valve and control valves at the cycle time of 30 min and the base-case operating conditions summarized in Table 2. Fig. 5a shows the inlet and outlet temperatures of the heating and cooling fluids before and after adsorber beds 1 and 2 as they are alternately heated and cooled for desorption and adsorption, respectively. Fig. 5 shows that control valves V5–V12 can repetitively direct the heating and cooling fluids to the adsorber beds. The pressures of the adsorber beds, $P_{bed,1}$ and $P_{bed,2}$, corresponding to adsorption and desorption are shown in Fig. 5b. It can be seen in Fig. 5b that the pressures of the adsorber beds vary between the condenser and evaporator pressures, P_{cond} and P_{evap}, where condensation and evaporation processes occur. Also, Fig. 5b indicates that whenever one of the adsorber beds undergoes the adsorption process, it is automatically connected to the evaporator via valves V1 or V3 and because of refrigerant evaporation in the evaporator, the chilled water outlet temperature, $T_{chilled,o}$, reduces. Fig. 5b also indicates that the expansion valve can provide the required pressure drop between the condenser and evaporator under the base-case operating conditions.

5.2. Parametric study

In this section, the performance of the ACS is studied under different operating conditions. In order to verify the numerical modeling, the SCP of ACS calculated from the numerical modeling is compared against that of calculated from the experimental data. Fig. 6 shows the effect of cycle time on the SCP of the ACS. As shown in Fig. 6, by increasing the cycle time from 20 to 30 min, the SCP increases by 177% from 3.3 to 9.15 W/kg. However, the SCP of ACS gradually reduces after the cycle time of 30 min because the adsorbate uptake capability of adsorbent particles reduces by increasing the cycle time. Fig. 6 shows that the model is capable of predicting the SCP of ACS with a good agreement for cycle times less than 30 min which are of the interest of vehicle applications [87].

Fig. 7 shows the effects of the heating and cooling fluid inlet temperatures on the SCP of the ACS. As shown in Fig. 7a, increasing the heating fluid inlet temperature to the adsorber beds from 70 to 100 °C increases the SCP from 0.7 to 14.8 W/kg. Increasing the temperature of the heating fluid to the adsorber beds during desorption causes faster heat transfer to the adsorbent material and, consequently, the rate of desorption of the adsorbate from the adsorbent material increases, and more adsorbate is desorbed. Accordingly, the drier adsorbent material adsorbs more adsorbate from the evaporator during the adsorption process. Therefore, higher cooling power

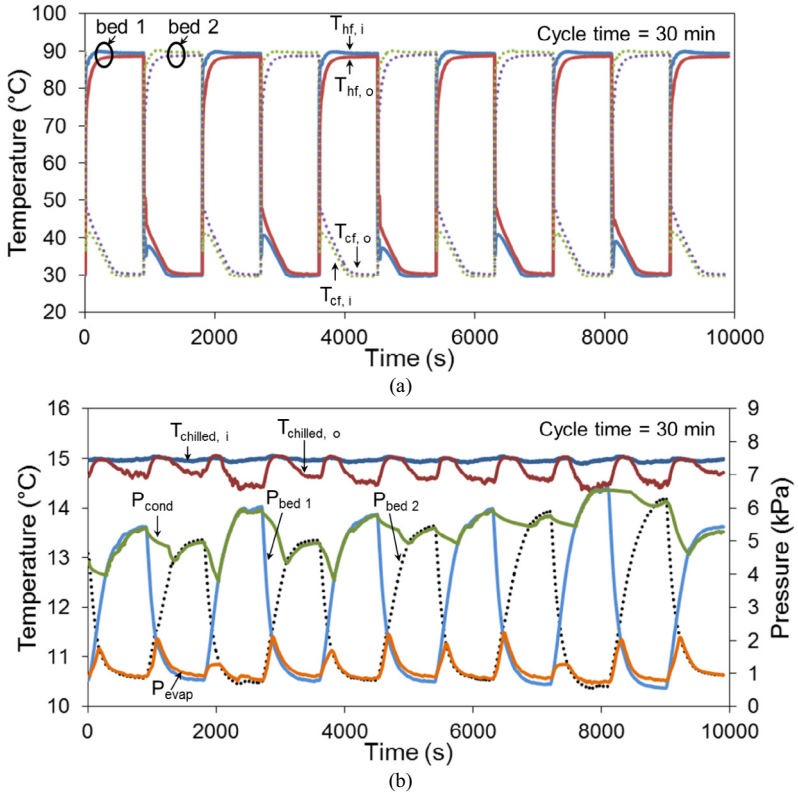

Fig. 5. The ACS performance under the base-case operating conditions summarized in Table 2. (a) Inlet and outlet temperatures of heating and cooling fluids pumped to the adsorber beds, and (b) operating pressures of the adsorber beds, condenser and evaporator, and chilled water inlet and outlet temperatures in the evaporator.

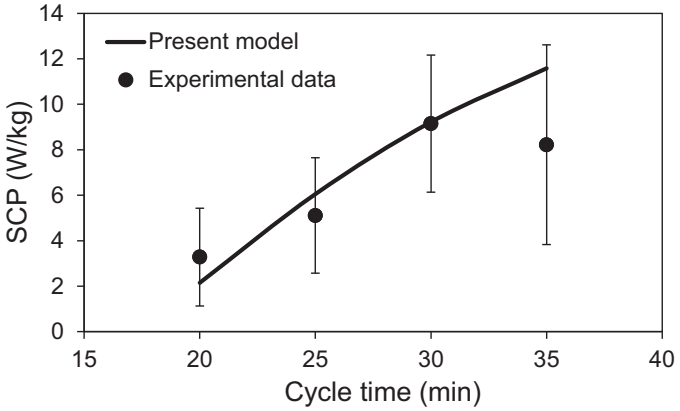

Fig. 6. Effects of cycle time on the SCP of the ACS. The operating conditions are kept constant at the base-case operating conditions summarized in Table 2.

(or SCP) is generated. In contrast, Fig. 7b shows that by increasing the cooling fluid inlet temperature from 30 to 40 °C, the SCP of the ACS reduces from 9.2 to 4.0 W/kg because higher adsorbent temperature during the adsorption process reduces the adsorbate uptake capacity of the adsorbent. Fig. 7 also depicts that the numerical modeling predicts the SCP of the ACS with good accuracy.

The effects of the coolant fluid inlet temperature circulated in the condenser on the SCP of ACS are shown in Fig. 8a. The SCP of the ACS decreases when the coolant fluid inlet temperature

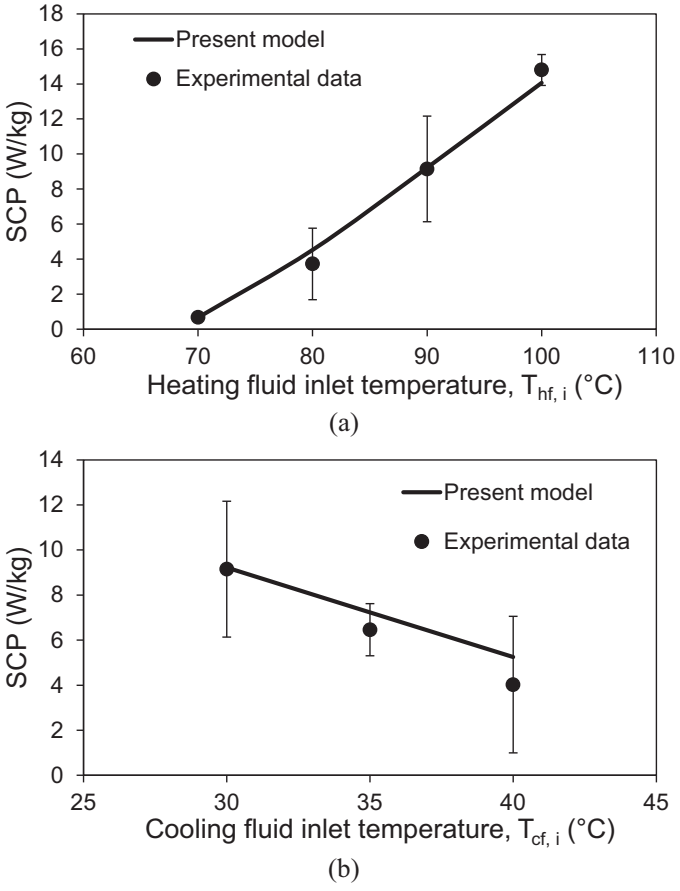

Fig. 7. Effects of (a) heating fluid and (b) cooling fluid inlet temperatures to the adsorber beds on the SCP of the ACS. The other operating conditions are kept constant at the base-case operating conditions summarized in Table 2.

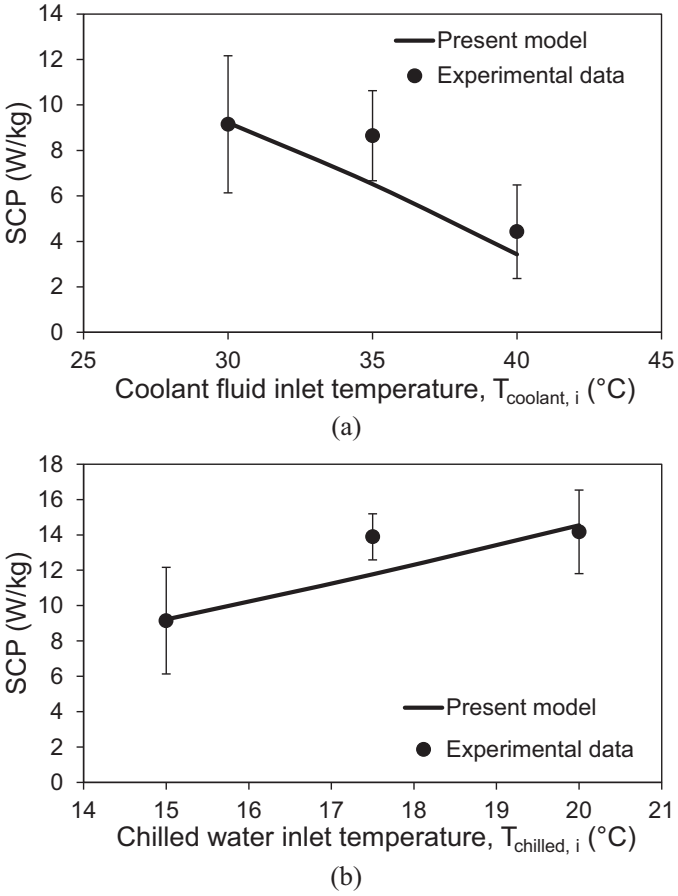

Fig. 8. Effects of (a) coolant fluid and (b) chilled water inlet temperatures pumped to the condenser and evaporator, respectively, on the SCP of the ACS. The other operating conditions are kept constant at the base-case operating conditions summarized in Table 2.

increases because of the increase in the condenser pressure and, as a result, lower amount of adsorbate condenses inside the condenser and adsorbent material dries less. Therefore, within a constant cycle time, lower adsorbate is desorbed from the adsorbent material and the adsorption capability of the adsorbent material during the adsorption process reduces. Fig. 8b demonstrates the effects of the chilled water inlet temperature flowing through the evaporator on the SCP of the ACS. As shown in Fig. 8b, by increasing the chilled water inlet temperature from 15 to 20 °C, the SCP of the ACS increases from 9.2 to 14.2 W/kg, i.e., a 54% increase, because the adsorbate uptake capability of the adsorbent material increases with the increasing the evaporator pressure during the adsorption process. Fig. 8 also displays that the numerical modeling is capable of predicting the SCP of the ACS with good accuracy.

5.3. Further improvement of the ACS

The parametric study indicates that the ideas proposed for the expansion and control valves of a waste heat-driven ACS can successfully operate under different operating conditions corresponding to what a light-duty vehicle A/C system experiences. However, the SCP of the designed ACS is not high enough because of low overall heat transfer conductance, $U_{bed}A_{bed}$, of the adsorber beds and, consequently, low heat transfer rate to the adsorbent material. Also, the evaporator and condenser designs should be changed to increase the evaporation and condensation rate. Using the verified numerical modeling, as an example, one can study the effects of an

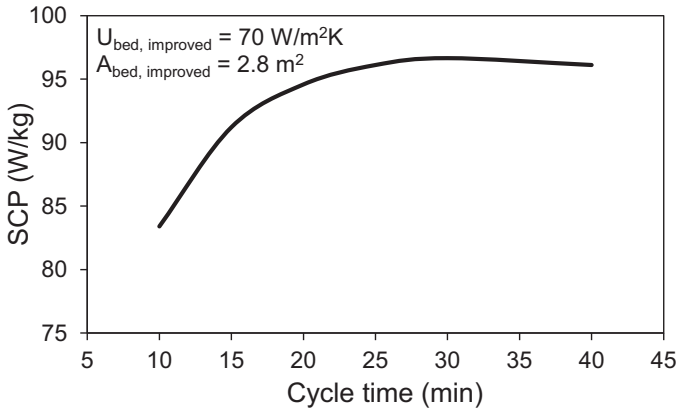

Fig. 9. Effect of cycle time on the SCP of the ACS calculated by the numerical modeling for an adsorber bed with $U_{bed}A_{bed}$ of 196 W/K. The other operating conditions are kept constant at the base-case operating conditions summarized in Table 2.

adsorber bed with higher heat transfer rate. To this end, reducing the fin spacing of the adsorber bed to increase the overall heat transfer coefficient, U_{bed}, and increasing the adsorber bed heat transfer surface area, A_{bed}, are practical solutions. Fig. 9 shows the SCP of the ACS with improved overall heat transfer conductance versus different cycle times. As shown in Fig. 9, increasing U_{bed} from 20 to 70 W/m²K, and A_{bed} from 0.235 to 2.8 m² result in the SCP of 83–96 W/kg within the cycle time 10–40 min.

6. Conclusion

In this study, new designs for the expansion valve and control valves of a waste heat-driven two-adsorber bed ACS were proposed and tested on a two-adsorber bed silica gel/$CaCl_2$-water ACS. The performance of the system was experimentally investigated under different operating conditions. The results showed that the expansion valve and control valves operated effectively in the system while the mass of the system was reduced by 10.5 kg and electricity power consumption of control valves was reduced by 50%. Also, a numerical model was developed and compared against the experimental data. The numerical results showed a good agreement with the experimental results under a wide range of operating conditions. The validated numerical model showed that by increasing the adsorber bed overall heat transfer coefficient and heat transfer surface area, the SCP of the ACS could be improved up to 6 times.

Acknowledgements

The first author thanks the LAEC members, Dr. Claire McCague, postdoctoral fellow, and Ms. Cecilia Berlanga, co-op student, for preparing silica gel/$CaCl_2$ required to run the experiments. Also, the authors gratefully acknowledge the financial support of the Natural Sciences and Engineering Research Council of Canada (NSERC) through the Automotive Partnership Canada Grant No. APCPJ 401826-10.

Nomenclature

A	Heat transfer surface area [m²]
A/C	Air conditioning
ACS	Adsorption cooling system
AAMR	Adsorber bed to adsorbent mass ratio [$kg_{metal}/kg_{dry\ adsorbent}$]
c	Heat capacity of solid materials [J/kg·K]
c_p	Heat capacity at constant pressure [J/kg·K]
COP	Coefficient of performance
D_s	Solid-side mass diffusivity [m²/s]
D_{s0}	Pre-exponential constant [m²/s]
E_a	Activation energy [J/mol]
Δh_{ads}	Enthalpy of adsorption [J/kg]
ΔT_{LM}	Log mean temperature difference [K]
h_{fg}	Enthalpy of vaporization [J/kg]
ICE	Internal combustion engine
M	Molar mass [kg/mol]
m	Mass [kg]
$\dot{m}$	Mass flow rate [kg/s]
P	Pressure [mbar]
Q_{total}	Total heat transfer [J]
$\dot{q}$	Heat transfer rate [W]
R_p	Average radius of adsorbent particles [m]
R_u	Universal gas constant [J/mol·K]
SCP	Specific cooling power [$W/kg_{dry\ adsorbent}$]
ω	Adsorbate uptake [$kg/kg_{dry\ adsorbent}$]
T	Temperature [K]
t	Time [s]
τ_{cycle}	Cycle time [s]
U	Overall heat transfer coefficient [W/m²·K]
VCRC	Vapor compression refrigeration cycle

Subscripts

adsorbate	Adsorbate
adsorbent	Adsorbent particles
bed	Adsorber bed
chilled	Chilled water
cf	Cooling fluid
cond	Condenser
coolant	Coolant fluid
cooling	Cooling process
eq	Equilibrium state
evap	Evaporator
heating	Heating process
hf	Heating fluid
i	In
liq.	Liquid phase
max	Maximum
min	Minimum
o	Out
sat	Saturation
vaporous	Vaporous phase

References

[1] M. Suzuki, Application of adsorption cooling systems to automobiles, Heat Recovery Syst. CHP 13 (1993) 335–340.
[2] M.O. Abdullah, I.A.W. Tan , L.S. Lim, Automobile adsorption air-conditioning system using oil palm biomass-based activated carbon: a review, Renew. Sustain. Energy Rev. 15 (2011) 2061–2072, doi:10.1016/j.rser.2011.01.012.
[3] H. Demir, M. Mobedi, S. Ülkü, A review on adsorption heat pump: problems and solutions, Renew. Sustain. Energy Rev. 12 (2008) 2381–2403, doi:10.1016/j.rser.2007.06.005.
[4] A. Sharafian, M. Bahrami, Assessment of adsorber bed designs in waste-heat driven adsorption cooling systems for vehicle air conditioning and refrigeration, Renew. Sustain. Energy Rev. 30 (2014) 440–451, doi:10.1016/j.rser.2013.10.031.
[5] A. Sharafian, M. Bahrami, Critical analysis of thermodynamic cycle modeling of adsorption cooling systems for light-duty vehicle air conditioning applications, Renew. Sustain. Energy Rev. 48 (2015) 857–869, doi:10.1016/j.rser.2015.04.055.
[6] G.E. Hulse, Freight car refrigeration by an adsorption system employing silica gel, Refrig. Eng. 17 (1929) 41–54.
[7] S. Jiangzhou, R.Z. Wang, Y.Z. Lu, Y.X. Xu, J.Y. Wu, Experimental investigations on adsorption air-conditioner used in internal-combustion locomotive driver-cabin, Appl. Therm. Eng. 22 (2002) 1153–1162, doi:10.1016/S1359-4311(02)00036-4.
[8] Y.Z. Lu, R.Z. Wang, S. Jianzhou, M. Zhang, Y. Xu, J. Wu, Performance of a diesel locomotive waste-heat-powered adsorption air conditioning system, Adsorption 10 (2004) 57–68.

[9] K. Wang, J.Y. Wu, R.Z. Wang, L.W. Wang, Composite adsorbent of CaCl2 and expanded graphite for adsorption ice maker on fishing boats, Int. J. Refrig. 29 (2006) 199–210, doi:10.1016/j.ijrefrig.2005.06.004.
[10] L.W. Wang, R.Z. Wang, Z.S. Lu, Y.X. Xu, J.Y. Wu, Split heat pipe type compound adsorption ice making test unit for fishing boats, Int. J. Refrig. 29 (2006) 456–468, doi:10.1016/j.ijrefrig.2005.08.007.
[11] Z.S. Lu, R.Z. Wang, T.X. Li, L.W. Wang, C.J. Chen, Experimental investigation of a novel multifunction heat pipe solid sorption icemaker for fishing boats using CaCl2/activated carbon compound–ammonia, Int. J. Refrig. 30 (2007) 76–85, doi:10.1016/j.ijrefrig.2006.07.001.
[12] K. Wang, J.Y. Wu, Z.Z. Xia, S.L. Li, R.Z. Wang, Design and performance prediction of a novel double heat pipes type adsorption chiller for fishing boats, Renew. Energy 33 (2008) 780–790, doi:10.1016/j.renene.2007.04.023.
[13] L.W. Wang, R.Z. Wang, Z.Z. Xia, J.Y. Wu, Studies on heat pipe type adsorption ice maker for fishing boats, Int. J. Refrig. 31 (2008) 989–997, doi:10.1016/j.ijrefrig.2008.01.002.
[14] R. De Boer, S.F. Smeding, Thermally operated mobile air-conditioning system: development and test of a laboratory prototype, in: International Sorption Heat Pump Conference, Seoul, Korea, 2008.
[15] R. De Boer, S.F. Smeding, S. Mola, Silicagel-water adsorption cooling prototype system for mobile air conditioning, in: Heat Powered Cycles Conference, Berlin, Germany, 2009.
[16] M. Verde, J.M. Corberan, R. de Boer, S. Smeding, Modelling of a waste heat driven silica gel/water adsorption cooling system comparison with experimental results, in: International Sorption Heat Pump, Padua, Italy, 2011, pp. 7–8.
[17] A. Sapienza, S. Santamaria, A. Frazzica, A. Freni, Influence of the management strategy and operating conditions on the performance of an adsorption chiller, Energy 36 (2011) 5532–5538, doi:10.1016/j.energy.2011.07.020.
[18] M. Pons, D. Laurent, F. Meunier, Experimental temperature fronts for adsorptive heat pump applications, Appl. Therm. Eng. 16 (1996) 395–404.
[19] F. Poyelle, J.J. Guilleminot, F. Meunier, Experimental tests and predictive model of an adsorptive air conditioning unit, Ind. Eng. Chem. Res. 38 (1999) 298–309, doi:10.1021/ie9802008.
[20] J.Y. Wu, R.Z. Wang, Y.X. Xu, Dynamic simulation and experiments of a heat regenerative adsorption heat pump, Energy Convers. Manag. 41 (2000) 1007–1018, doi:10.1016/S0196-8904(99)00161-2.
[21] R.Z. Wang, J.Y. Wu, Y.X. Xu, W. Wang, Performance researches and improvements on heat regenerative adsorption refrigerator and heat pump, Energy Convers. Manag. 42 (2001) 233–249, doi:10.1016/S0196-8904(99)00189-2.
[22] R.Z. Wang, Performance improvement of adsorption cooling by heat and mass recovery operation, Int. J. Refrig. 24 (2001) 602–611.
[23] R.Z. Wang, Adsorption refrigeration research in Shanghai Jiao Tong University, Renew. Sustain. Energy Rev. 5 (2001) 1–37.
[24] T.F. Qu, R.Z. Wang, W. Wang, Study on heat and mass recovery in adsorption refrigeration cycles, Appl. Therm. Eng. 21 (2001) 439–452, doi:10.1016/S1359-4311(00)00050-8.
[25] J.Y. Wu, R.Z. Wang, Y.X. Xu, Experimental results on operating parameters influence for an adsorption refrigerator, Int. J. Therm. Sci. 41 (2002) 137–145.
[26] Y.B. Gui, R.Z. Wang, W. Wang, J.Y. Wu, Y.X. Xu, Performance modeling and testing on a heat-regenerative adsorptive reversible heat pump, Appl. Therm. Eng. 22 (2002) 309–320, doi:10.1016/S1359-4311(01)00082-5.
[27] D. Wang, J. Wu, H. Shan, R. Wang, Experimental study on the dynamic characteristics of adsorption heat pumps driven by intermittent heat source at heating mode, Appl. Therm. Eng. 25 (2005) 927–940, doi:10.1016/j.applthermaleng.2004.07.013.
[28] D. Wang, J. Wu, Influence of intermittent heat source on adsorption ice maker using waste heat, Energy Convers. Manag. 46 (2005) 985–998, doi:10.1016/j.enconman.2004.06.002.
[29] R.G. Oliveira, V. Silveira, R.Z. Wang, Experimental study of mass recovery adsorption cycles for ice making at low generation temperature, Appl. Therm. Eng. 26 (2006) 303–311, doi:10.1016/j.applthermaleng.2005.04.021.
[30] Z. Tamainot-Telto, R.E. Critoph, Monolithic carbon for sorption refrigeration and heat pump applications, Appl. Therm. Eng. 21 (2001) 37–52, doi:10.1016/S1359-4311(00)00030-2.
[31] R.E. Critoph, Simulation of a continuous multiple-bed regenerative adsorption cycle, Int. J. Refrig. 24 (2001) 428–437.
[32] R.E. Critoph, Multiple bed regenerative adsorption cycle using the monolithic carbon–ammonia pair, Appl. Therm. Eng. 22 (2002) 667–677, doi:10.1016/S1359-4311(01)00118-1.
[33] Z. Tamainot-Telto, R.E. Critoph, Advanced solid sorption air conditioning modules using monolithic carbon–ammonia pair, Appl. Therm. Eng. 23 (2003) 659–674, doi:10.1016/S1359-4311(02)00238-7.
[34] R.E. Critoph, Adsorption refrigeration research at Warwick, in: 1st TECCS Meeting, 2007.
[35] R.E. Critoph, S.J. Metcalf, Specific cooling power intensification limits in ammonia–carbon adsorption refrigeration systems, Appl. Therm. Eng. 24 (2004) 661–678, doi:10.1016/j.applthermaleng.2003.11.004.
[36] R.E. Critoph, Y. Zhong, Review of trends in solid sorption refrigeration and heat pumping technology, Proc. Inst. Mech. Eng. E J. Process. Mech. Eng. 219 (2005) 285–300, doi:10.1243/095440805X6982.
[37] Z. Tamainot-Telto, S.J. Metcalf, R.E. Critoph, Novel compact sorption generators for car air conditioning, Int. J. Refrig. 32 (2009) 727–733, doi:10.1016/j.ijrefrig.2008.11.010.
[38] S.J. Metcalf, Z. Tamainot-Telto, R.E. Critoph, Application of a compact sorption generator to solar refrigeration: case study of Dakar (Senegal), Appl. Therm. Eng. 31 (2011) 2197–2204, doi:10.1016/j.applthermaleng.2010.11.001.
[39] X. Wang, H.T. Chua, K.C. Ng, Experimental investigation of silica gel–water adsorption chillers with and without a passive heat recovery scheme, Int. J. Refrig. 28 (2005) 756–765, doi:10.1016/j.ijrefrig.2004.11.011.
[40] A. Akahira, K.C.A. Alam, Y. Hamamoto, A. Akisawa, T. Kashiwagi, Mass recovery four-bed adsorption refrigeration cycle with energy cascading, Appl. Therm. Eng. 25 (2005) 1764–1778, doi:10.1016/j.applthermaleng.2004.10.006.
[41] K.C.A. Alam, M.Z.I. Khan, A.S. Uyun, Y. Hamamoto, A. Akisawa, T. Kashiwagi, Experimental study of a low temperature heat driven re-heat two-stage adsorption chiller, Appl. Therm. Eng. 27 (2007) 1686–1692, doi:10.1016/j.applthermaleng.2006.07.006.
[42] Y.L. Liu, R.Z. Wang, Z.Z. Xia, Experimental performance of a silica gel–water adsorption chiller, Appl. Therm. Eng. 25 (2005) 359–375, doi:10.1016/j.applthermaleng.2004.06.012.
[43] Y.L. Liu, R.Z. Wang, Z.Z. Xia, Experimental study on a continuous adsorption water chiller with novel design, Int. J. Refrig. 28 (2005) 218–230, doi:10.1016/j.ijrefrig.2004.09.004.
[44] D.C. Wang, Z.Z. Xia, J.Y. Wu, Design and performance prediction of a novel zeolite–water adsorption air conditioner, Energy Convers. Manag. 47 (2006) 590–610, doi:10.1016/j.enconman.2005.05.011.
[45] A. Akahira, K.C.A. Alam, Y. Hamamoto, A. Akisawa, T. Kashiwagi, Experimental investigation of mass recovery adsorption refrigeration cycle, Int. J. Refrig. 28 (2005) 565–572, doi:10.1016/j.ijrefrig.2004.10.001.
[46] W.S. Chang, C.-C. Wang, C.-C. Shieh, Experimental study of a solid adsorption cooling system using flat-tube heat exchangers as adsorption bed, Appl. Therm. Eng. 27 (2007) 2195–2199, doi:10.1016/j.applthermaleng.2005.07.022.
[47] R.E. Critoph, Towards a one tonne per day solar ice maker, Renew. Energy 9 (1996) 626–631, doi:10.1016/0960-1481(96)88366-2.
[48] Z. Tamainot-Telto, R.E. Critoph, Adsorption refrigerator using monolithic carbon-ammonia pair, Int. J. Refrig. 20 (1997) 146–155.
[49] R.E. Critoph, Rapid cycling solar/biomass powered adsorption refrigeration system, Renew. Energy 16 (1999) 673–678.
[50] K. Oertel, M. Fischer, Adsorption cooling system for cold storage using methanol/silicagel, Appl. Therm. Eng. 18 (1998) 773–786, doi:10.1016/S1359-4311(97)00107-5.
[51] L.Z. Zhang, L. Wang, Momentum and heat transfer in the adsorbent of a waste-heat adsorption cooling system, Energy 24 (1999) 605–624, doi:10.1016/S0360-5442(99)00018-3.
[52] L.Z. Zhang, L. Wang, Effects of coupled heat and mass transfers in adsorbent on the performance of a waste heat adsorption cooling unit, Appl. Therm. Eng. 19 (1999) 195–215.
[53] L.Z. Zhang, Design and testing of an automobile waste heat adsorption cooling system, Appl. Therm. Eng. 20 (2000) 103–114, doi:10.1016/S1359-4311(99)00009-5.
[54] G. Restuccia, A. Freni, S. Vasta, Y.I. Aristov, Selective water sorbent for solid sorption chiller: experimental results and modelling, Int. J. Refrig. 27 (2004) 284–293, doi:10.1016/j.ijrefrig.2003.09.003.
[55] D. Magnetto, Thermally Operated Mobile Air Conditioning Systems, 2005.
[56] D.C. Wang, Z.Z. Xia, J.Y. Wu, R.Z. Wang, H. Zhai, W.D. Dou, Study of a novel silica gel–water adsorption chiller. Part I. Design and performance prediction, Int. J. Refrig. 28 (2005) 1073–1083, doi:10.1016/j.ijrefrig.2005.03.001.
[57] D.C. Wang, J.Y. Wu, Z.Z. Xia, H. Zhai, R.Z. Wang, W.D. Dou, Study of a novel silica gel–water adsorption chiller. Part II. Experimental study, Int. J. Refrig. 28 (2005) 1084–1091, doi:10.1016/j.ijrefrig.2005.03.002.
[58] D.C. Wang, Z.X. Shi, Q.R. Yang, X.L. Tian, J.C. Zhang, J.Y. Wu, Experimental research on novel adsorption chiller driven by low grade heat source, Energy Convers. Manag. 48 (2007) 2375–2381, doi:10.1016/j.enconman.2007.03.001.
[59] G. Restuccia, A. Freni, F. Russo, S. Vasta, Experimental investigation of a solid adsorption chiller based on a heat exchanger coated with hydrophobic zeolite, Appl. Therm. Eng. 25 (2005) 1419–1428, doi:10.1016/j.applthermaleng.2004.09.012.
[60] G.Z. Yang, Z.Z. Xia, R.Z. Wang, D. Keletigui, D.C. Wang, Z.H. Dong, et al., Research on a compact adsorption room air conditioner, Energy Convers. Manag. 47 (2006) 2167–2177, doi:10.1016/j.enconman.2005.12.005.
[61] L.W. Wang, R.Z. Wang, Z.S. Lu, C.J. Chen, J.Y. Wu, Comparison of the adsorption performance of compound adsorbent in a refrigeration cycle with and without mass recovery, Chem. Eng. Sci. 61 (2006) 3761–3770, doi:10.1016/j.ces.2006.01.018.
[62] Z.S. Lu, R.Z. Wang, L.W. Wang, C.J. Chen, Performance analysis of an adsorption refrigerator using activated carbon in a compound adsorbent, Carbon N. Y. 44 (2006) 747–752, doi:10.1016/j.carbon.2005.09.016.
[63] L.W. Wang, R.Z. Wang, Z.S. Lu, C.J. Chen, K. Wang, J.Y. Wu, The performance of two adsorption ice making test units using activated carbon and a carbon composite as adsorbents, Carbon N. Y. 44 (2006) 2671–2680, doi:10.1016/j.carbon.2006.04.013.
[64] C.J. Chen, R.Z. Wang, L.W. Wang, Z.S. Lu, Studies on cycle characteristics and application of split heat pipe adsorption ice maker, Energy Convers. Manag. 48 (2007) 1106–1112, doi:10.1016/j.enconman.2006.10.017.
[65] A. Freni, F. Russo, S. Vasta, M. Tokarev, Y.I. Aristov, G. Restuccia, An advanced solid sorption chiller using SWS-1L, Appl. Therm. Eng. 27 (2007) 2200–2204, doi:10.1016/j.applthermaleng.2005.07.023.
[66] K. Daou, R.Z. Wang, Z.Z. Xia, G.Z. Yang, Experimental comparison of the sorption and refrigerating performances of a CaCl2 impregnated composite adsorbent

and those of the host silica gel, Int. J. Refrig. 30 (2007) 68–75, doi:10.1016/j.ijrefrig.2006.05.003.
[67] Y.I. Aristov, A. Sapienza, D.S. Ovoshchnikov, A. Freni, G. Restuccia, Reallocation of adsorption and desorption times for optimisation of cooling cycles, Int. J. Refrig. 35 (2012) 525–531, doi:10.1016/j.ijrefrig.2010.07.019.
[68] A. Sapienza, I.S. Glaznev, S. Santamaria, A. Freni, Y.I. Aristov, Adsorption chilling driven by low temperature heat: new adsorbent and cycle optimization, Appl. Therm. Eng. 32 (2012) 141–146, doi:10.1016/j.applthermaleng.2011.09.014.
[69] A. Freni, A. Sapienza, I.S. Glaznev, Y.I. Aristov, G. Restuccia, Experimental testing of a lab-scale adsorption chiller using a novel selective water sorbent "silica modified by calcium nitrate", Int. J. Refrig. 35 (2012) 518–524, doi:10.1016/j.ijrefrig.2010.05.015.
[70] L.X. Gong, R.Z. Wang, Z.Z. Xia, C.J. Chen, Design and performance prediction of a new generation adsorption chiller using composite adsorbent, Energy Convers. Manag. 52 (2011) 2345–2350, doi:10.1016/j.enconman.2010.12.036.
[71] Z.S. Lu, R.Z. Wang, Study of the new composite adsorbent of salt LiCl/silica gel–methanol used in an innovative adsorption cooling machine driven by low temperature heat source, Renew. Energy 63 (2014) 445–451, doi:10.1016/j.renene.2013.10.010.
[72] Z.S. Lu, R.Z. Wang, Z.Z. Xia, Q.B. Wu, Y.M. Sun, Z.Y. Chen, An analysis of the performance of a novel solar silica gel–water adsorption air conditioning, Appl. Therm. Eng. 31 (2011) 3636–3642, doi:10.1016/j.applthermaleng.2010.11.024.
[73] Z. Lu, R. Wang, Z. Xia, L. Gong, Experimental investigation adsorption chillers using micro-porous silica gel–water and compound adsorbent-methanol, Energy Convers. Manag. 65 (2013) 430–437, doi:10.1016/j.enconman.2012.09.018.
[74] Z.S. Lu, R.Z. Wang, Performance improvement and comparison of mass recovery in CaCl 2/activated carbon adsorption refrigerator and silica gel/LiCl adsorption chiller driven by low grade waste heat, Int. J. Refrig. 36 (2013) 1504–1511, doi:10.1016/j.ijrefrig.2013.03.008.
[75] S. Vasta, A. Freni, A. Sapienza, F. Costa, G. Restuccia, Development and lab-test of a mobile adsorption air-conditioner, Int. J. Refrig. 35 (2012) 701–708, doi:10.1016/j.ijrefrig.2011.03.013.
[76] J. Wang, L.W. Wang, W.L. Luo, R.Z. Wang, Experimental study of a two-stage adsorption freezing machine driven by low temperature heat source, Int. J. Refrig. 36 (2013) 1029–1036, doi:10.1016/j.ijrefrig.2012.10.029.
[77] F.P. Song, L.X. Gong, L.W. Wang, R.Z. Wang, Study on gradient thermal driven adsorption cycle with freezing and cooling output for food storage, Appl. Therm. Eng. 70 (2014) 231–239, doi:10.1016/j.applthermaleng.2014.04.066.
[78] J.K. Kiplagat, R.Z. Wang, R.G. Oliveira, T.X. Li, M. Liang, Experimental study on the effects of the operation conditions on the performance of a chemisorption air conditioner powered by low grade heat, Appl. Energy 103 (2013) 571–580, doi:10.1016/j.apenergy.2012.10.025.
[79] J.-Y. San, F.-K. Tsai, Testing of a lab-scale four-bed adsorption heat pump, Appl. Therm. Eng. 70 (2014) 274–281, doi:10.1016/j.applthermaleng.2014.05.014.
[80] Q.W. Pan, R.Z. Wang, Z.S. Lu, L.W. Wang, Experimental investigation of an adsorption refrigeration prototype with the working pair of composite adsorbent-ammonia, Appl. Therm. Eng. 72 (2014) 275–282, doi:10.1016/j.applthermaleng.2014.06.054.
[81] C.Y. Tso, K.C. Chan, C.Y.H. Chao, C.L. Wu, Experimental performance analysis on an adsorption cooling system using zeolite 13X/CaCl2 adsorbent with various operation sequences, Int. J. Heat Mass Transf. 85 (2015) 343–355, doi:10.1016/j.ijheatmasstransfer.2015.02.005.
[82] A. Sharafian, M. Bahrami, A quasi steady state model for adsorption cooling systems: automotive applications, in: ASME 2012 6th International Conference Energy Sustainability. 10th Fuel Cell Science, Engineering and Technology Conference, San Diego, CA, USA, 2012.
[83] A. Sharafian, C. McCague, M. Bahrami, Impact of fin spacing on temperature distribution in adsorption cooling system for vehicle A/C applications, Int. J. Refrig. 51 (2015) 135–143.
[84] R.J.H. Grisel, S.F. Smeding, R. de Boer, Waste heat driven silica gel/water adsorption cooling in trigeneration, Appl. Therm. Eng. 30 (2010) 1039–1046, doi:10.1016/j.applthermaleng.2010.01.020.
[85] Y.I. Aristov, I.S. Glaznev, A. Freni, G. Restuccia, Kinetics of water sorption on SWS-1L (calcium chloride confined to mesoporous silica gel): influence of grain size and temperature, Chem. Eng. Sci. 61 (2006) 1453–1458, doi:10.1016/j.ces.2005.08.033.
[86] B.B. Saha, A. Chakraborty, S. Koyama, Y.I. Aristov, A new generation cooling device employing $CaCl_2$-in-silica gel–water system, Int. J. Heat Mass Transf. 52 (2009) 516–524, doi:10.1016/j.ijheatmasstransfer.2008.06.018.
[87] M.A. Lambert, B.J. Jones, Automotive adsorption air conditioner powered by exhaust heat. Part 1: conceptual and embodiment Design, Proc. Inst. Mech. Eng. D J. Automob. Eng. 220 (2006) 959–972, doi:10.1243/09544070JAUTO221.